

# Hole-doping-induced changes in the electronic structure of $\text{La}_{1-x}\text{Sr}_x\text{FeO}_3$ : soft x-ray photoemission and absorption study of epitaxial thin films

H. Wadati,<sup>1</sup> D. Kobayashi,<sup>2</sup> H. Kumigashira,<sup>2</sup> K. Okazaki,<sup>1</sup> T. Mizokawa,<sup>1</sup> A. Fujimori,<sup>1</sup>  
K. Horiba,<sup>2</sup> M. Oshima,<sup>2</sup> N. Hamada,<sup>3</sup> M. Lippmaa,<sup>4</sup> M. Kawasaki,<sup>5</sup> and H. Koinuma<sup>6</sup>

<sup>1</sup>*Department of Physics and Department of Complexity Science and Engineering,  
University of Tokyo, Bunkyo-ku, Tokyo 113-0033, Japan*

<sup>2</sup>*Department of Applied Chemistry, University of Tokyo, Bunkyo-ku, Tokyo 113-8656, Japan*

<sup>3</sup>*Department of Physics, Tokyo University of Science, 2641 Yamazaki, Noda, Chiba 278-8510, Japan*

<sup>4</sup>*Institute for Solid State Physics, University of Tokyo,  
Kashiwanoha 5-1-5, Kashiwa, Chiba 277-8581, Japan*

<sup>5</sup>*Institute for Materials Research, Tohoku University, 2-1-1 Katahira, Aoba, Sendai 980-8577, Japan*

<sup>6</sup>*Materials and Structures Laboratory, Tokyo Institute of Technology 4259 Nagatsuta, Midori-ku, Yokohama 226-8503, Japan*

(Dated: October 18, 2018)

We have studied the electronic structure of epitaxially grown thin films of  $\text{La}_{1-x}\text{Sr}_x\text{FeO}_3$  by *in-situ* photoemission spectroscopy (PES) and x-ray absorption spectroscopy (XAS) measurements. The Fe 2*p* and valence-band PES spectra and the O 1*s* XAS spectra of  $\text{LaFeO}_3$  have been successfully reproduced by configuration-interaction cluster-model calculation and, except for the satellite structure, by band-structure calculation. From the shift of the binding energies of core levels, the chemical potential was found to be shifted downward as  $x$  was increased. Among the three peaks in the valence-band spectra of  $\text{La}_{1-x}\text{Sr}_x\text{FeO}_3$ , the peak nearest to the Fermi level ( $E_F$ ), due to the “ $e_g$  band”, was found to move toward  $E_F$  and became weaker as  $x$  was increased, whereas the intensity of the peak just above  $E_F$  in the O 1*s* XAS spectra increased with  $x$ . The gap or pseudogap at  $E_F$  was seen for all values of  $x$ . These results indicate that changes in the spectral line shape around  $E_F$  are dominated by spectral weight transfer from below to above  $E_F$  across the gap and are therefore highly non-rigid-band-like.

PACS numbers: 71.28.+d, 71.30.+h, 79.60.Dp, 73.61.-r

## I. INTRODUCTION

Since the discovery of high- $T_c$  superconductivity in the cuprates, great interest has revived in perovskite-type transition-metal oxides because of their intriguing properties, such as metal-insulator transition (MIT), colossal magnetoresistance (CMR), and ordering of spin, charge, and orbitals [1]. In most cases, hole doping plays a crucial role in realizing these interesting physical properties. However, there has been little consensus on how the electronic structure evolves with hole doping in these compounds, namely, whether new states are created in the gap or the chemical potential is simply shifted as in the rigid-band model, even in the most extensively studied case of the high- $T_c$  cuprates [2, 3, 4]. Among the perovskite-type transition-metal oxides,  $\text{La}_{1-x}\text{Sr}_x\text{FeO}_3$  (LSFO) has attracted much interest because it undergoes a pronounced charge disproportionation and an associated MIT around  $x \simeq 2/3$  [5]. One end member,  $\text{LaFeO}_3$ , is an antiferromagnetic insulator with a high Néel temperature ( $T_N = 738$  K). The character of the band gap is of the charge-transfer (CT) type, and the optical gap is  $\sim 2.1$  eV [6]. The other end member,  $\text{SrFeO}_3$ , is a helical antiferromagnetic metal with  $T_N = 134$  K. In an early photoemission study, it was found that its ground state is dominated by the  $d^5\bar{\underline{L}}$  configuration, where  $\bar{\underline{L}}$  denotes a hole in the O 2*p* band, rather than the  $d^4$  configuration [7], meaning that the system is a negative-charge-transfer-energy compound and that holes in the oxygen

2*p* band are responsible for the metallic behavior [8, 9]. One striking feature of LSFO is that the insulating phase is unusually wide in the phase diagram (especially at low temperatures  $0 < x < 0.9$ , and even at room temperature  $0 < x < 0.5$ ) [10]. The O 1*s* x-ray absorption spectroscopy (XAS) study by Abbate *et al.* [11] has suggested that doped holes have the O 2*p* character. Therefore, the central question for this system remains unresolved of how does the electronic structure evolve from a CT insulator  $\text{LaFeO}_3$  to the metallic oxygen holes of  $\text{SrFeO}_3$  as a function of hole doping.

Recently, high-quality perovskite-type oxide single-crystal thin films grown by pulsed laser deposition (PLD) have become available [12, 13], and a setup has been developed for their *in-situ* photoemission measurement [14, 15]. In the present work, we address the above questions about the electronic structure of LSFO by measuring soft x-ray photoemission and absorption spectra of epitaxially-grown high-quality thin films prepared *in situ*. A systematic x-ray photoemission study of scraped bulk LSFO samples has been reported by Chainani *et al.* [16]. Structures in the valence band, however, were not clearly resolved partly because of the limited energy resolution ( $\sim 0.8$  eV). In a more recent study by Matsuno *et al.* using similarly prepared samples [10], detailed temperature-dependent changes near the Fermi level ( $E_F$ ) were studied with high energy resolution. However, the O 2*p* cross section overwhelmed the Fe 3*d* emission for the low photon energies  $20 \lesssim h\nu \lesssim 100$  eV

used in their study [17].

In the present study, we have used soft x-rays with high-energy resolution ( $\sim 200$  meV) and succeeded in resolving detailed spectral features and in directly obtaining more information about the Fe  $3d$  states. We could determine the Fe  $3d$  contribution more clearly with better bulk sensitivity due to the longer photoelectron escape depth for the higher photoelectron kinetic energies [18]. We emphasize that in the present work the usefulness of bulk sensitivity is further enhanced by the use of high-quality epitaxial thin film samples [14]. Combining the soft x-ray photoemission spectra and O  $1s$  XAS spectra, we have successfully obtained a picture of how the electronic structure evolves from a CT insulator to an oxygen-hole metal through the observation of the chemical potential shift and spectral weight transfer.

## II. EXPERIMENT

The photoemission spectroscopy (PES) and XAS measurements were performed at BL-2C of Photon Factory, High Energy Accelerators Research Organization (KEK), using a combined Laser molecular beam epitaxy (MBE) and photoemission spectrometer system. Details of the experimental setup are described in Ref [15]. Epitaxial films of LSFO were fabricated by the PLD method. Single crystals of Nb-doped SrTiO<sub>3</sub> were used as substrates. Nb-doping was necessary to avoid charging effects during the PES measurements. A Nd:YAG laser was used for ablation in its frequency-tripled mode ( $\lambda = 355$  nm) at a repetition rate of 0.33 Hz. The substrates were annealed at 1050°C at an oxygen pressure of  $\sim 1 \times 10^{-6}$  Torr to obtain an atomically flat TiO<sub>2</sub>-terminated surface [19]. LSFO thin films of  $\sim 100$  monolayers were deposited on the substrates at 950°C at an oxygen pressure of  $\sim 1 \times 10^{-4}$  Torr. The films were post-annealed at 400°C at an atmospheric pressure of oxygen to remove oxygen vacancies. The samples were then transferred from the MBE chamber to the spectrometer under ultrahigh vacuum. The surface morphology of the measured films was checked by *ex-situ* atomic force microscopy (AFM). The AFM image of a LaFeO<sub>3</sub> thin film in Fig. 1 shows atomically flat step-and-terrace structures. The crystal structure was characterized by four-circle X-ray diffraction, and coherent growth on the substrate was observed. All the photoemission measurements were performed under an ultrahigh vacuum of  $\sim 10^{-10}$  Torr at room temperature. The PES spectra were measured using a Scienta SES-100 electron-energy analyzer. The total energy resolution was about 200-500 meV depending on photon energy. The Fermi level ( $E_F$ ) position was determined by measuring gold spectra. The XAS spectra were measured using the total-electron-yield method.

The stoichiometry of thin films was carefully characterized by analyzing the relative intensity of the relevant core levels, confirming that the composition of samples is almost the same as ceramic targets.

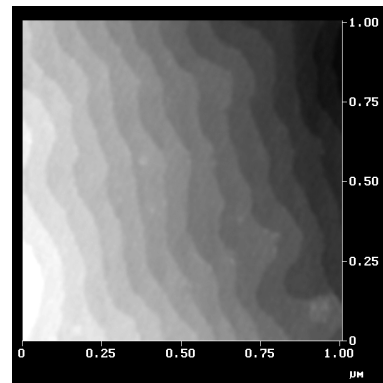


FIG. 1: AFM image of an epitaxially grown LaFeO<sub>3</sub> thin film. Image size is  $1 \mu\text{m} \times 1 \mu\text{m}$ .

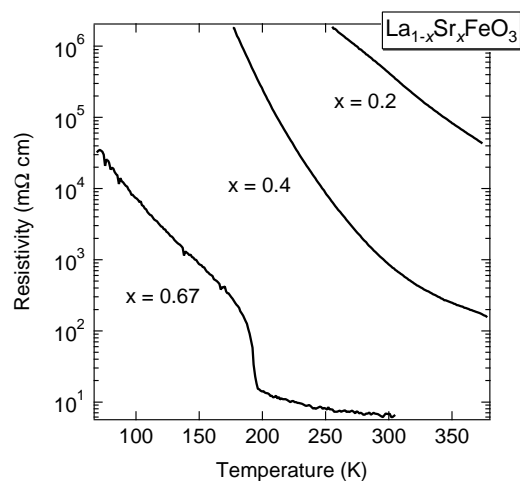


FIG. 2: Electrical resistivity of La<sub>1-x</sub>Sr<sub>x</sub>FeO<sub>3</sub> thin films.

## III. RESULTS AND DISCUSSION

### A. Electrical resistivities

Figure 2 shows the electrical resistivity of La<sub>1-x</sub>Sr<sub>x</sub>FeO<sub>3</sub> thin films samples which were made under the same condition as the samples for the photoemission measurements. The samples for the resistivity measurements were grown on Nb-free SrTiO<sub>3</sub> substrates to prevent the electric current from flowing through the conducting substrate. As for  $x = 0.67$ , there is a jump of resistivity, caused by charge disproportionation, almost at the same temperature as the bulk samples [10, 20] ( $T_{CD} = 190$  K). [35]

### B. LaFeO<sub>3</sub>

Before proceeding to the composition dependence of LSFO, we first characterize the electronic structure of the

La-end composition, LaFeO<sub>3</sub> (LFO). Figure 3 gives the Fe 2*p* PES spectrum, the valence-band PES spectrum, and the O 1*s* XAS spectrum of LFO. As the  $E_F$  position for O 1*s* XAS cannot be determined unambiguously from the O 1*s* core-level PES and XAS data because of the unknown effect of the core-hole potential [21], the XAS spectrum has been aligned so that the gap magnitude agrees with that obtained from the optical measurements, 2.1 eV [6], as shown in Fig. 3 (b). In the main valence-band region  $[-(0 - 10)$  eV], we observe three structures denoted by A, B, and C and a satellite structure at  $\sim -12$  eV. Structure A is assigned to the  $e_g$  states of Fe 3*d*, structure B to the  $t_{2g}$  states, and structure C to the Fe 3*d* - O 2*p* bonding states. The O 1*s* XAS spectrum shows empty Fe 3*d* states within  $\sim 5$  eV of  $E_F$  and the La 5*d* states above it. The empty Fe 3*d* states are split into two peaks, D and E, due to the  $e_g - t_{2g}$  crystal-field splitting.

In order to interpret those spectra quantitatively, we performed a configuration-interaction (CI) cluster-model calculation [7, 22]. We considered an [FeO<sub>6</sub>]<sup>9-</sup> octahedral cluster. In this model, the ground state is described as

$$\Psi_g = \alpha_1|d^5\rangle + \alpha_2|d^6\bar{L}\rangle + \alpha_3|d^7\bar{L}^2\rangle + \dots \quad (1)$$

Our model, in which  $d$  electrons are assumed to be localized in the cluster, is considered to be a good approximation since LaFeO<sub>3</sub> is an insulator and the LDA+ $U$  calculation has shown that the Fe 3*d* states in LaFeO<sub>3</sub> have weak band dispersion, so the translational symmetry does not affect the angle-integrated photoemission spectra of the Fe 3*d* band significantly. The final state for the emission of an Fe 2*p* core electron is given by

$$\Psi_f = \beta_1|\underline{c}d^5\rangle + \beta_2|\underline{c}d^6\bar{L}\rangle + \beta_3|\underline{c}d^7\bar{L}^2\rangle + \dots, \quad (2)$$

where  $\underline{c}$  denotes an Fe 2*p* core hole. The final state for the emission of an Fe 3*d* electron is given by

$$\Psi_f = \gamma_1|d^4\rangle + \gamma_2|d^5\bar{L}\rangle + \gamma_3|d^6\bar{L}^2\rangle + \dots, \quad (3)$$

and that for O 1*s* XAS by

$$\Psi_f = \delta_1|d^6\rangle + \delta_2|d^7\bar{L}\rangle + \delta_3|d^8\bar{L}^2\rangle + \dots \quad (4)$$

The O 1*s* XAS spectrum represents the unoccupied O 2*p* partial DOS, and since other orbitals are strongly hybridized with the O 2*p* orbitals, O 1*s* XAS also reflects the empty Fe 3*d* and La 5*d* bands.

To calculate the valence-band PES spectrum, the O 2*p* emission spectrum has to be added to the Fe 3*d* spectrum. The line shape of the O 2*p* band was taken from the PES data of La<sub>0.33</sub>Sr<sub>0.67</sub>FeO<sub>3</sub>, measured at  $h\nu = 21.2$  eV [23]. In order to take into account the chemical potential shift between LaFeO<sub>3</sub> and La<sub>0.33</sub>Sr<sub>0.67</sub>FeO<sub>3</sub> (see Fig. 6), the  $h\nu = 21.2$  eV spectrum has been shifted downward by 0.78 eV. The relative intensities of the Fe 3*d* - and O 2*p* - derived spectra have been determined from the atomic photoionization cross sections [17] with the O 2*p* intensity multiplied by a factor of  $\sim 3$  [24]. Parameters

to be fitted are the charge-transfer energy from the O 2*p* orbitals to the empty Fe 3*d* orbitals denoted by  $\Delta$ , the 3*d* - 3*d* on-site Coulomb interaction energy denoted by  $U$ , and the hybridization strength between the Fe 3*d* and O 2*p* orbitals denoted by Slater-Koster parameters ( $pd\sigma$ ) and ( $pd\pi$ ). The ratio  $(pd\sigma)/(pd\pi) = -2.2$  has been assumed, as usual [7, 22]. The configuration dependence of the transfer integrals has been taken into account [25]. Racah parameters are fixed at the free ion values of Fe<sup>3+</sup> ( $B = 0.126$  eV,  $C = 0.595$  eV) [26]. We took into account the intra-atomic multiplet coupling for the valence-band spectrum, whereas it was not taken fully into account for the Fe 2*p* spectrum as in the case of [7].

The calculated Fe 2*p* core-level photoemission spectrum has been broadened with an energy-dependent Lorentzian with FWHM

$$2\Gamma = 2\Gamma_0(1 + \alpha\Delta E), \quad (5)$$

where  $\Delta E$  denotes the energy separation from the main peak. We adopted the values  $\alpha = 0.15$  and  $\Gamma_0 = 1.2$  eV. We then used a Gaussian broadening of 1.0 eV to simulate the instrumental resolution and broadening due to the core hole-3*d* multiplet coupling. The calculated valence-band spectrum has been broadened with a Gaussian of 1.6 eV FWHM and an energy-dependent Lorentzian (FWHM =  $0.2|E - E_F|$  eV) [27] to account for the combined effects of the instrumental resolution and the  $d$  band dispersion, and the lifetime broadening of the photohole, respectively.

The best-fit results have been obtained setting  $\Delta = 2.0$  eV,  $U = 6.0$  eV, and  $(pd\sigma) = -1.9$  eV as shown in Fig. 3. The  $e_g - t_{2g}$  crystal-field parameter of  $10Dq = 0.41$  eV was assumed to reproduce the splitting in the O 1*s* XAS spectrum. These parameters are consistent with previously reported ones, which showed that LaFeO<sub>3</sub> is a charge-transfer-type insulator, where  $\Delta < U$  [7]. However, the value of  $U$  had to be taken smaller than the previously reported value ( $U = 7.5$  eV) [7] in order to reproduce both the Fe 2*p* core level and valence-band spectra simultaneously. As we have succeeded in reproducing both the core level and the valence band using the same parameter set, the present results are more accurate than previous ones [7], although the PES spectrum calculated with this  $U$  value is still slightly too deep and the band gap is overestimated as shown in Fig. 3 (b). Also, there is a significant difference in the calculated and the experimental satellite energy positions. For the Fe 2*p* spectrum, we conclude that the main peaks mostly come from  $\underline{c}d^6\bar{L}$  and  $\underline{c}d^7\bar{L}^2$  final states, while there is significant contribution of the  $\underline{c}d^5$  final states to the satellite. Good agreement is obtained between the calculated and the experimental satellite energy position, in contrast to the valence band. As mentioned above, the effect of the intra-atomic multiplet is treated differently in the core-level and valence-band CI calculations, and this point probably causes this difference. Therefore, the precise agreement of the satellite position of the core-level spectrum may be rather fortuitous. For the valence band,

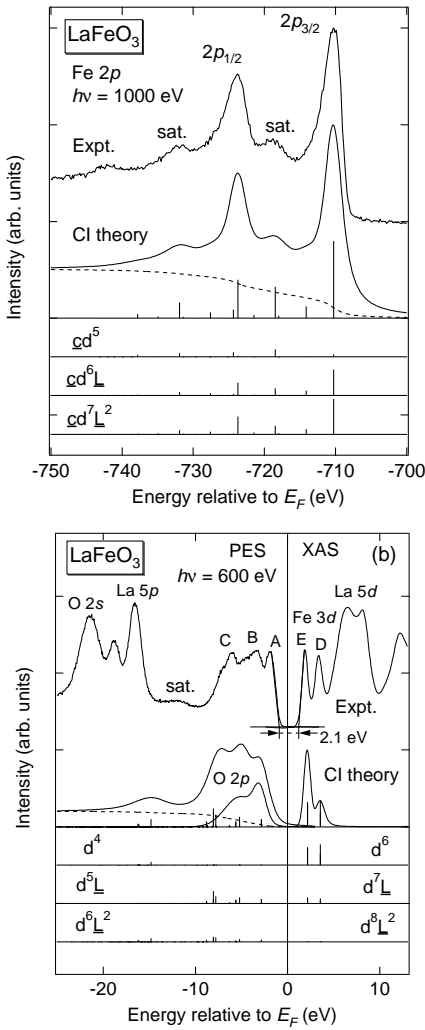


FIG. 3: Photoemission and XAS spectra of  $\text{LaFeO}_3$  and their CI cluster-model analyses. In the bottom panels, final states are decomposed into contributions from different configurations. The dotted lines indicate the background due to secondary electrons. (a) Fe 2p core-level photoemission spectrum. (b) Valence-band photoemission and O 1s XAS spectra.

we conclude that the three main structures are derived from  $d^5\bar{L}$  and  $d^6\bar{L}^2$  final states with admixture of the O 2p band, while the satellite has strong contribution from the  $d^4$  final state. Due to the small value of  $\Delta$ , final states with two holes at the ligand site are important for the interpretation of the PES spectra. As for the O 1s XAS spectrum, the final states have mostly  $d^6$  character, and therefore one can interpret the data without significant contributions from charge-transfer ( $d^7\bar{L}$ ,  $d^8\bar{L}^2$ , ...) final states.

We have also compared the spectra with the LDA + $U$  band-structure calculation in Fig. 4. The full-potential linearized augmented-plane-wave (FLAPW) method was employed with an exchange-correlation po-

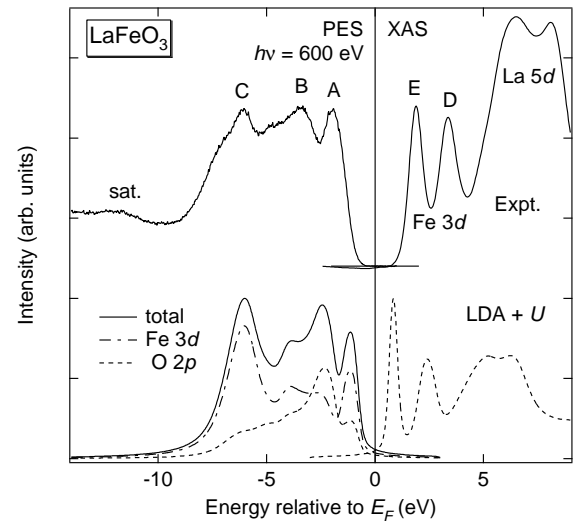


FIG. 4: Comparison of the photoemission and O 1s XAS spectra of  $\text{LaFeO}_3$  with the LDA + $U$  band-structure calculation.

tential of Vosko, Wilk and Nusair [28]. The effective Coulomb interaction parameter,  $U_{eff} \equiv U - J$ , in the LDA + $U$  scheme was set to 2 eV for all the Fe 3d orbitals [29]. A G-type antiferromagnetic state was assumed. The calculated DOS has been broadened with a Gaussian of 0.15 eV FWHM and an energy-dependent Lorentzian (FWHM =  $0.2|E - E_F|$  eV) [27] to account for the instrumental resolution and the lifetime broadening of the photohole, respectively. Below  $E_F$ , we have added the partial DOS of O  $p$  and Fe  $d$ , considering their cross sections at  $h\nu = 600$  eV [17], with the multiplication factor of  $\sim 3$  for the O  $p$  partial DOS [24]. Above  $E_F$ , we have considered only the partial DOS of O  $p$  because the O 1s XAS spectrum is due to the dipole-allowed transition from the O 1s core level. The three main structures, A, B, and C, were successfully reproduced (including a weak shoulder between B and C), consistent with a previous report [30]. However, the calculated band gap of 1.3 eV was too small compared with the optical gap of 2.1 eV [6], and the satellite structure could not be reproduced since our value of  $U_{eff} = 2$  eV was chosen to be the best value for the reproduction of the main structures, not of the satellite structure and the value of the band gap.

From this comparison, we conclude that the valence-band spectra of LFO can be explained well both by the CI cluster-model calculation and, except for the satellite structure, by the LDA + $U$  band-structure calculation. It is a reasonable result that both calculations can reproduce the Fe 3d - band region of  $\text{LaFeO}_3$  equally well because, except for the satellite, there is one-to-one correspondence between the two calculations for the peak positions and the orbital character for the  $e_g$  band (structure-A),  $t_{2g}$  band (structure-B), and Fe 3d - O 2p bonding states (structure-C).

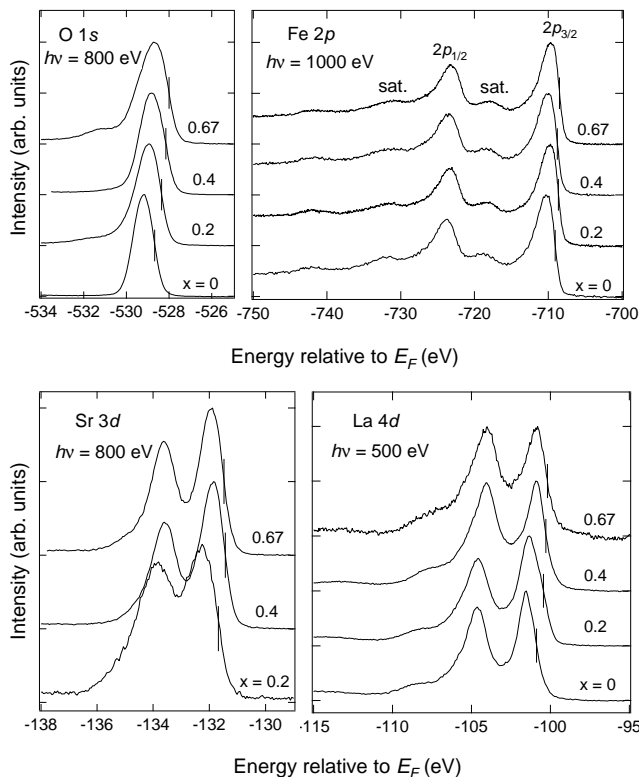


FIG. 5: Core-level photoemission spectra of  $\text{La}_{1-x}\text{Sr}_x\text{FeO}_3$ .

### C. $\text{La}_{1-x}\text{Sr}_x\text{FeO}_3$

Next, we go to the question of how the electronic structure of LFO changes upon hole doping. Figure 5 shows the core-level photoemission spectra of  $\text{La}_{1-x}\text{Sr}_x\text{FeO}_3$ . The “contamination” signal on the higher binding energy side of the O 1s peak was weak enough, except for the  $x = 0.67$  sample, indicating that the surface was reasonably clean. The line shape of the Fe 2p core level has almost no composition dependence, consistent with the picture that doped holes go into states of primarily O 2p character, and not of Fe 3d character [11].

All the core-level spectra, except for the Fe 2p core level, are shifted toward lower binding energies with  $x$ , as plotted in Fig. 6 (a). Here, the midpoint of the lower binding energy slope is taken as representing the shift of the peaks because this part is generally least affected by possible contamination [31, 32]. In determining the “Relative energy”, we adopted the sample of  $x = 0.4$  as the zero. The sample of  $x = 0$  has no Sr, so we cannot adopt this as the zero. We consider that it is reasonable to adopt  $x = 0.4$  as the zero since  $x = 0.4$  is almost in the mid-position of this hole-doping system although it is not the unique choice.

The shift  $\Delta E_B$  of a core-level binding energy measured from  $\mu$  is given by

$$\Delta E_B = \Delta\mu + K\Delta Q + \Delta V_M + \Delta E_R, \quad (6)$$

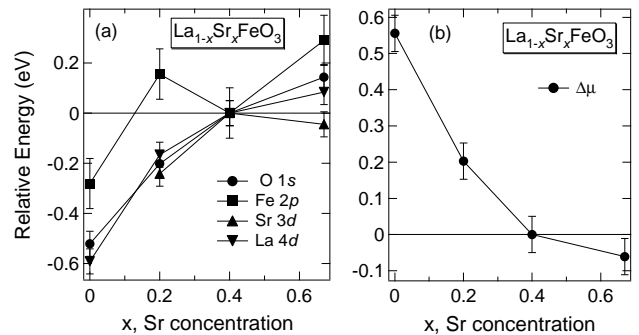


FIG. 6: Binding energy shifts of spectral features in  $\text{La}_{1-x}\text{Sr}_x\text{FeO}_3$ . (a) Core levels. (b) Chemical potential shift deduced from the O 1s, Sr 3d, and La 4d core levels.

where  $\Delta\mu$  is the change in the chemical potential,  $\Delta Q$  is the change in the number of valence electrons on the atom considered,  $\Delta V_M$  is the change in the Madelung potential, and  $\Delta E_R$  is the change in the core-hole screening [33]. As seen in Fig. 6 (a) the Fe 2p core level moves in a different way from the other core levels probably because the formal valence of Fe changes with hole doping, reflecting both the chemical potential shift and the “chemical shift”, which is due to the increase in the Fe valence with hole doping ( $\propto -\Delta Q$ ), as in other transition-metal oxides [31, 32, 34]. The similar shifts of the O 1s, Sr 3d, and La 4d core levels indicate that the change in the Madelung potential ( $\Delta V_M$ ) is negligibly small because it would shift the core levels of anions and cations in different directions. Core-hole screening by conduction electrons is also considered to be negligibly small in transition-metal oxides [31, 32, 34]. Therefore, we take the average of the shifts of these three core levels as a measure of  $\Delta\mu$  in LSFO. Figure 6 (b) shows  $\Delta\mu$  thus determined plotted as a function of  $x$ . The shifts become slightly weaker above  $x = 0.4$ . In the rigid band picture,  $-\partial\mu/\partial x$  is inversely proportional to the DOS at  $E_F$  [34], which may explain the weakening of the chemical potential shift. However, there is a gap (absence of finite DOS at  $E_F$ ) or a pseudogap (depression of DOS at  $E_F$ , see Fig. 7 (a)) for all the compositions, which means that interpretation beyond the rigid band picture is necessary.  $\text{La}_{2-x}\text{Sr}_x\text{CuO}_4$  is a typical example in which the suppression of the chemical potential shift has been observed in the underdoped region, where there is a pseudogap at  $E_F$  [31]. This phenomenon has been attributed to the formation of charge stripes, a kind of “microscopic phase separation” in which the distance between hole stripes decreases with hole concentration  $x$ . Further studies up to  $x = 1$  are necessary to see whether the weakening of the shifts at large  $x$ 's is related to the charge disproportionation or not.

Figure 7 (a) shows the doping dependence of the combined valence-band photoemission and the O 1s XAS spectra. Here, the Fermi levels of the XAS spectra for

various  $x$  have been determined by combining the Fermi level position in the LFO spectrum with the  $x$ -dependent shift of the O  $1s$  core-level peak for the sake of convenience [36]. In the PES spectra, one can observe the three main structures A ( $e_g$  band), B ( $t_{2g}$  band), and C (Fe  $3d - O 2p$  bonding states) and the satellite, as in the case of LFO. A gap (absence of finite DOS at  $E_F$ ) or a pseudogap (depression of DOS at  $E_F$ ) was seen for all values of  $x$ , as was observed for  $\text{La}_{1-x}\text{Sr}_x\text{MnO}_3$  [21]. The sample of  $x = 0.67$  undergoes a metal-insulator transition at 190 K, but there is little DOS at  $E_F$  at room temperature. This may be related to the fact that the electrical resistivity satisfies  $d\rho/dT < 0$  even above the transition temperature as shown in Fig. 2. The intensity of the satellite has almost no composition dependence. Figure 7 (b) shows the binding energy shifts of structures A, B, and C plotted against  $x$ . Structures A-C move toward  $E_F$  upon hole doping up to  $x = 0.4$ . These shifts are in good agreement with the core level shifts, indicating the rigid-band shift occurs in the valence band. In addition, structure A, which is assigned to the “ $e_g$  band”, becomes weaker with increasing  $x$ , indicating that holes are doped into the “ $e_g$  band”, and is finally obscured at  $x = 0.67$ . The weakening of structure A with  $x$  is more clearly seen in Fig. 7 (c), where the energy positions of structures B and C have been aligned. In the XAS spectra, a new peak F grows within the band gap of LFO upon hole doping, as seen in the previous study [11]. Since  $x = 0, 0.2, 0.4$  samples are insulating, structure A and F are separated by a gap. Therefore, this structure F cannot be part of structure A but a state created in the gap. The combined PES and XAS spectra thus demonstrate that spectral weight is transferred from structure A below  $E_F$  to structure F above  $E_F$ , and the band gap is filled by the new spectral weight F as holes are doped. Spectral weight of structures A and F is plotted as a function of Sr concentration  $x$  in Fig. 7 (d). The weight of structure F is almost proportional to  $x$ , indicating that doped holes go into this structure. Also,  $E_F$  is located within the gap or the pseudogap for all  $x$ 's, that is, the intensity at  $E_F$  remains always small (more clearly in the PES spectrum), which may correspond to the wide insulating region in the LSFO phase diagram. This non-rigid-band behavior within  $\sim 2$  eV of  $E_F$  is apparently in conflict with the monotonic chemical potential shift. We therefore conclude that in this system the effect of hole-doping can be described in the framework of the rigid-band model as far as the shifts of the spectral features are concerned, whereas the “ $e_g$  band” shows highly non-rigid-band-like behavior with transfer of spectral weight from below  $E_F$  to above it across the gap or pseudogap at  $E_F$ .

#### IV. CONCLUSION

We have studied the composition-dependent electronic structures of LSFO using epitaxial thin films by *in-situ* PES and XAS measurements. By using soft x-rays of

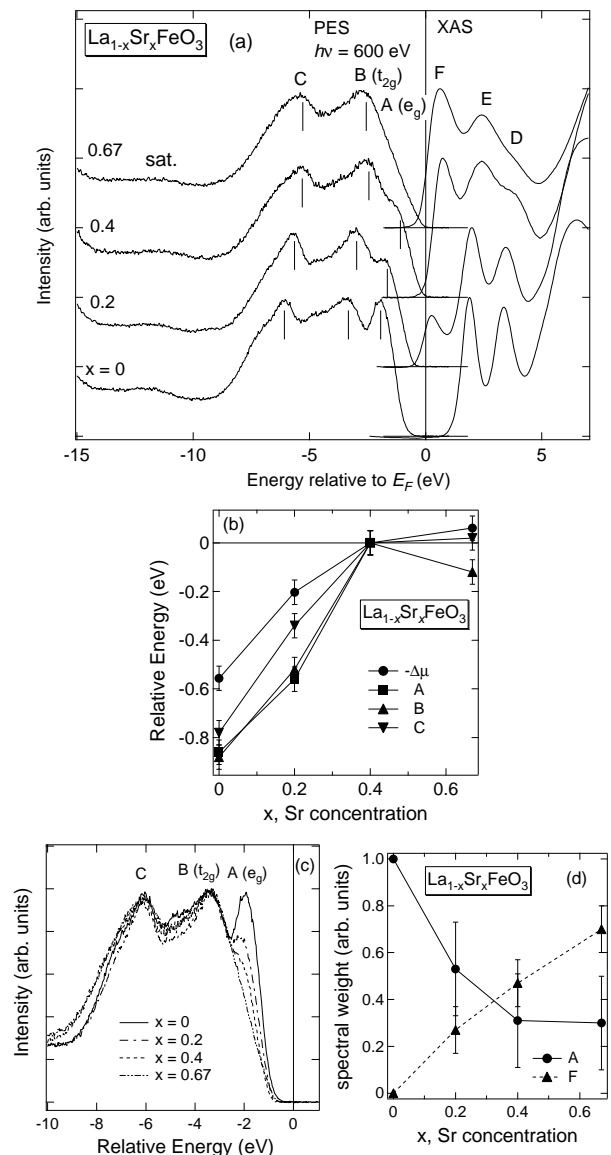


FIG. 7: PES and XAS spectra of  $\text{La}_{1-x}\text{Sr}_x\text{FeO}_3$ . (a) Combined PES and XAS spectra. (b) Shifts of structures in the valence band. (c) Valence-band photoemission spectra shifted so that structures A, B, and C are aligned. (d) Spectral weight of structures A and F as functions of  $x$ .

high energy resolution and high-quality sample surfaces, we succeeded in obtaining high-quality spectra with detailed spectral features of high bulk sensitivity. The Fe  $2p$  and valence-band PES spectra and the O  $1s$  XAS spectra of  $\text{LaFeO}_3$  have been successfully reproduced by CI cluster-model calculation as well as by band-structure calculation. This is considered to be a natural result because there is a one-to-one correspondence between both calculations for the structures in the valence band. The shift of the chemical potential was found to become slightly weak above  $x = 0.4$ . Further studies up to  $x = 1$  are necessary to see whether this weakening is related to

the charge disproportionation around  $x = 0.67$ . In the valence-band spectra, the structure nearest to  $E_F$  becomes weaker and moves toward  $E_F$  as  $x$  is increased. The gap or pseudogap at  $E_F$  was seen for all compositions. These results mean that the simple rigid band model does not work in this system and the transfer of spectral weight occurs across  $E_F$  in a highly non-rigid-band-like manner.

## V. ACKNOWLEDGMENT

The authors would like to thank A. Tanaka for informative discussions. We are also grateful to K. Ono and

A. Yagishita for their support at KEK-PF. This work was done under the approval of the Photon Factory Program Advisory Committee (Proposal No. 2003G149) and under Project No. 2002S2-002 at the Institute of Material Structure Science, KEK.

- 
- [1] M. Imada, A. Fujimori, and Y. Tokura, *Rev. Mod. Phys.* **70**, 1039 (1998).
- [2] M. A. van Veenendaal, R. Schlattmann, G. A. Sawatzky, and W. A. Groen, *Phys. Rev. B* **47**, 446 (1993).
- [3] H. Eisaki, S. Uchida, T. Mizokawa, H. Namatame, A. Fujimori, J. van Elp, P. Kuiper, G. A. Sawatzky, S. Hosoya, and H. Katayama-Yoshida, *Phys. Rev. B* **45**, 12513 (1992).
- [4] C. T. Chen, F. Sette, Y. Ma, M. S. Hybertsen, E. B. Stechel, W. M. C. Foulkes, M. Schluter, S.-W. Cheong, A. S. Cooper, L. W. Rupp, B. Batlogg, Y. L. Soo, Z. H. Ming, A. Krol, and Y. H. Kao, *Phys. Rev. Lett.* **66**, 104 (1991).
- [5] M. Takano, J. Kawachi, N. Nakanishi, and Y. Takeda, *J. Solid. State Chem.* **39**, 75 (1981).
- [6] T. Arima, Y. Tokura, and J. B. Torrance, *Phys. Rev. B* **48**, 17006 (1993).
- [7] A. E. Bocquet, A. Fujimori, T. Mizokawa, T. Saitoh, H. Namatame, S. Suga, N. Kimizuka, Y. Takeda, and M. Takano, *Phys. Rev. B* **45**, 1561 (1992).
- [8] T. Mizokawa, H. Namatame, A. Fujimori, K. Akeyama, H. Kondoh, H. Kuroda, and N. Kosugi, *Phys. Rev. Lett.* **67**, 1638 (1991).
- [9] T. Kawakami, S. Nasu, K. Kuzushita, T. Sasaki, S. Morimoto, T. Yamada, S. Endo, S. Kawasaki, and M. Takano, *J. Phys. Soc. Jpn.* **72**, 33 (2003).
- [10] J. Matsuno, T. Mizokawa, A. Fujimori, K. Mamiya, Y. Takeda, S. Kawasaki, and M. Takano, *Phys. Rev. B* **60**, 4605 (1999).
- [11] M. Abbate, F. M. F. de Groot, J. C. Fuggle, A. Fujimori, O. Strelbel, F. Lopez, M. Domke, G. Kaindl, G. A. Sawatzky, M. Takano, Y. Takeda, H. Eisaki, and S. Uchida, *Phys. Rev. B* **46**, 4511 (1992).
- [12] M. Izumi, Y. Konishi, T. Nishihara, S. Hayashi, M. Shinohara, M. Kawasaki, and Y. Tokura, *Appl. Phys. Lett.* **73**, 2497 (1998).
- [13] J. Choi, C. B. Eom, G. Rijnders, H. Rogalla, and D. H. A. Blank, *Appl. Phys. Lett.* **79**, 1447 (2001).
- [14] H. Kumigashira, K. Horiba, H. Oguchi, K. Ono, M. Oshima, N. Nakagawa, M. Lippmaa, M. Kawasaki, and H. Koinuma, *Appl. Phys. Lett.* **82**, 3430 (2003).
- [15] K. Horiba, H. Oguchi, H. Kumigashira, M. Oshima, K. Ono, N. Nakagawa, M. Lippmaa, M. Kawasaki, and H. Koinuma, *Rev. Sci. Instr.* **74**, 3406 (2003).
- [16] A. Chainani, M. Mathew, and D. D. Sarma, *Phys. Rev. B* **48**, 14818 (1993).
- [17] J. J. Yeh and I. Lindau, *At. Data Nucl. Data Tables* **32**, 1 (1985).
- [18] A. Sekiyama, T. Iwasaki, K. Matsuda, Y. Saitoh, Y. Onuki, and S. Suga, *Nature* **403**, 396 (2000).
- [19] M. Kawasaki, K. Takahashi, T. Maeda, R. Tsuchiya, M. Shinohara, O. Ishihara, T. Yonezawa, M. Yoshimoto, and H. Koinuma, *Science* **266**, 1540 (1994).
- [20] T. Ishikawa, S. K. Park, T. Katsufuji, T. Arima, and Y. Tokura, *Phys. Rev. B* **58**, R13326 (1998).
- [21] T. Saitoh, A. E. Bocquet, T. Mizokawa, H. Namatame, A. Fujimori, M. Abbate, Y. Takeda, and M. Takano, *Phys. Rev. B* **51**, 13942 (1995).
- [22] A. Fujimori and F. Minami, *Phys. Rev. B* **30**, 957 (1984).
- [23] J. Matsuno (unpublished).
- [24] G. A. Sawatzky and D. Post, *Phys. Rev. B* **20**, 1546 (1979).
- [25] T. Mizokawa and A. Fujimori, *Phys. Rev. B* **48**, 14150 (1993).
- [26] Y. Tanabe and S. Sugano, *J. Phys. Soc. Jpn.* **9**, 766 (1954).
- [27] H. Höchst, P. Steiner, G. Reiter, and S. Hüfner, *Z. Phys. B* **42**, 199 (1981).
- [28] S. H. Vosko, L. Wilk, and M. Nusair, *Can. J. Phys.* **58**, 1200 (1980).
- [29] I. Solovyev, N. Hamada, and K. Terakura, *Phys. Rev. B* **53**, 7158 (1996).
- [30] D. D. Sarma, N. Shanthi, S. R. Barman, N. Hamada, H. Sawada, and K. Terakura, *Phys. Rev. Lett.* **75**, 1126 (1995).
- [31] A. Ino, T. Mizokawa, A. Fujimori, K. Tamasaku, H. Eisaki, S. Uchida, T. Kimura, T. Sasagawa, and K. Kishio, *Phys. Rev. Lett.* **79**, 2101 (1997).
- [32] J. Matsuno, A. Fujimori, Y. Takeda, and M. Takano, *Europhys. Lett.* **59**, 252 (2002).
- [33] S. Hüfner, *Photoelectron Spectroscopy* (Springer-Verlag, Berlin, 1995).
- [34] A. Fujimori, A. Ino, J. Matsuno, T. Yoshida, K. Tanaka, and T. Mizokawa, *J. Electron Spectrosc. Relat. Phenom.* **124**, 127 (2002).
- [35] This transition is often called “metal-insulator transition”, but the electrical resistivity satisfies  $d\rho/dT < 0$  even above the transition temperature.

[36] It has been recognized for many years that XAS spectra, in particular O  $1s$  XAS in transition-metal oxides, do not precisely represent unoccupied DOS and also that it is difficult to determine the exact  $E_F$  position. For example, the BIS spectra (K. Morikawa *et al.*, Phys. Rev. B 52, 13711 (1995)) and the O  $1s$  XAS spectra (H. I. Inoue *et al.*, Physica C 235-240 1007 (1994)) of  $\text{CaVO}_3$

and  $\text{SrVO}_3$  are different. The O  $1s$  XAS spectra show a build-up of spectral weight at the leading edge, which is not present in the real DOS measured by BIS. Therefore, the tail of the XAS spectra of the doped samples does not necessarily mean that the DOS is finite at  $E_F$ .